SoftwareX 18 (2022) 101011

Contents lists available at ScienceDirect

SoftwareX

journal homepage: www.elsevier.com/locate/softx

Original software publication

2PJIT: Two-phase 3D jet instability tool in cylindrical coordinates

Mohan Ananth, Mario F. Trujillo *

Department of Mechanical Engineering, University of Wisconsin-Madison, Madison, WI 53706, United States of America

ARTICLE INFO

Article history:
Received 22 June 2021
Received in revised form 24 January 2022
Accepted 28 January 2022

Keywords:
Linear stability analysis
Spatial stability
Two-phase flows

ABSTRACT

The two-phase 3D jet spatial instability tool (2PJIT) is a generalized Matlab-based software used to predict the growth of instabilities in two-phase shear flows involving cylindrical jets. The software solves the Linearized Navier–Stokes equation via the Chebyshev spectral method in both the liquid and gas phase along with the interfacial constraints. For a given set of input frequencies, the software outputs the corresponding wavenumbers, the associated eigen-vector/function, and the spatial growth rate for radial, azimuthal, and axial disturbances.

Current code version	v1
Permanent link to code/repository used for this code version	https://github.com/ElsevierSoftwareX/SOFTX-D-21-00119
Code Ocean compute capsule	none
Legal Code License	Apache-2.0 License
Code versioning system used	none
Software code languages, tools, and services used	MatLab-2017a-2020b
Compilation requirements, operating environments & dependencies	none
If available Link to developer documentation/manual	none
Support email for questions	mananth2@wisc.edu, mtrujillo@wisc.edu

1. Motivation and significance

A ubiquitous hydrodynamic stability problem occurring in various gas–liquid flows involves two fluid streams moving at different velocities separated by a gas–liquid interface, $\Gamma(t)$. Some of the applications include falling liquid films over a vertically oriented surface [1], waves on the water surface created by winds [2], and liquid jet injection and atomization [3,4]. A common approach used to study these problems is through linear stability analysis (LSA). One of the early studies on instabilities was done by [5] which has been extended over the years to varying geometries and conditions [6].

While there has been a large number of LSA studies over decades, there have been relatively few open-source codes published, which can be used to solve the underlying system of equations. Of those large number of studies, only a very limited group considers three-dimensional instabilities in cylindrical geometries [7]. And out of this small group, there are *no published codes* to the authors' knowledge. The present work is aimed at addressing this absence since flows under cylindrical geometries play a central role in various applications involving the use of liquid injection to create a spray or simply to disperse liquid [4].

The current tool solves the linearized Navier–Stokes equation for two-phase, cylindrical coordinates involving *spatially* growing disturbances, with interfacial constraints involving the continuity of the velocity fields and the jump conditions. Both axisymmetric and asymmetric modes of the disturbances are considered. The resulting eigenvalue differential equation is solved using the spectral method involving Chebyshev polynomials. For the given set of input frequencies, this tool outputs the corresponding unstable wavenumber and their spatial growth rates, along with the perturbation velocity and pressure fields. The accuracy of the solver is ensured by monitoring the residual errors of the equations being solved.

* Corresponding author.
E-mail address: mtrujillo@wisc.edu (Mario F. Trujillo).

https://doi.org/10.1016/j.softx.2022.101011

2. Mathematical description of system

The following material provides a succinct description of the system of equations solved in the code beginning with the governing equations 2.1, interfacial and boundary conditions 2.2, and normal mode representation 2.3, and spectral discretization 2.4.

2.1. Governing equations

The governing equations are the Navier–Stokes, the continuity equation for an *incompressible* flow, and the interfacial constraints along with appropriate boundary conditions. Adopting a cylindrical geometry, the velocity and pressure fields are decomposed in terms of their base flow and perturbed counterparts as follows

$$\begin{aligned}\mathbf{u}^q(r,\theta,z,t) &= \mathbf{U}^q(r) + \mathbf{u}'^q(r,\theta,z,t)\\ &= \left[0,0,U_z^q(r)\right]\\ &\quad + \left[u_r'^q(r,\theta,z,t), u_\theta'^q(r,\theta,z,t), u_z'^q(r,\theta,z,t)\right] \quad (1a)\end{aligned}$$

$$p^q(r,\theta,z,t) = P^q(r) + p'^q(r,\theta,z,t). \quad (1b)$$

where (r,θ,z,t) are the radial, azimuthal, axial, and temporal coordinates respectively. Superscript q denotes fields or properties belonging to either the liquid or gas domain, i.e. $q = L$ or $q = G$, respectively. Furthermore, the *base flow* variables are $U_z^q(r)$ and $P^q(r)$ and the corresponding *perturbed flow* components are $u_r'^q(r,\theta,z,t)$, $u_\theta'^q(r,\theta,z,t)$, $u_z'^q(r,\theta,z,t)$, and $p'^q(r,\theta,z,t)$. A visual representation of the system to be solved along with a representation of the instabilities and domain considered are depicted in Fig. 1.

Substituting Eqs. (1) into the continuity and momentum equation and ignoring second order contributions from the perturbed quantities yields

$$\nabla \cdot \mathbf{u}'^{\mathbf{q}} = 0 \quad \text{and} \quad (2a)$$

$$\frac{\partial \mathbf{u}'^{\mathbf{q}}}{\partial t} + \mathbf{U}^{\mathbf{q}} \cdot \nabla \mathbf{u}'^{\mathbf{q}} + \mathbf{u}'^{\mathbf{q}} \cdot \nabla \mathbf{U}^{\mathbf{q}} = -\frac{1}{\rho^q}\nabla p'^q + \nu^q \nabla^2 \mathbf{u}'^{\mathbf{q}}. \quad (2b)$$

where ρ and ν are the density and kinematic viscosity, respectively. The governing equations are subsequently non-dimensionalized by incorporating the undisturbed jet radius, R, the jet velocity, U_{jet}, and the advection time, R/U_{jet}. The resulting Reynolds number is defined as $Re = \rho_L U_{jet} R/\mu_L$.

2.2. Boundary and interfacial conditions

The boundary conditions for velocity and pressure at the liquid centerline ($r = 0$) depend on whether the disturbance is axisymmetric or asymmetric instabilities. These boundary conditions are combined with the far-field condition at $r = H$. Both sets are given by

At $r = 0$ (Axisymmetric):

$$u_r' = 0 \quad ; \quad u_\theta' = 0 \quad ; \quad \frac{\partial u_z'}{\partial r} = 0 \quad ; \quad \frac{\partial p'}{\partial r} = 0. \quad (3a)$$

At $r = 0$ (Asymmetric):

$$\frac{\partial u_r'}{\partial r} = 0 \quad ; \quad u_r' + \frac{\partial u_\theta'}{\partial \theta} = 0 \quad ; \quad u_z' = 0 \quad ; \quad p' = 0. \quad (3b)$$

At $r = H$:

$$u_r' = 0 \quad ; \quad u_\theta' = 0 \quad ; \quad \frac{\partial u_z'}{\partial r} = 0 \quad ; \quad \frac{\partial p'}{\partial r} = 0. \quad (3c)$$

The second set of conditions are imposed at the gas–liquid interface and constitute the interfacial constraints given by

Continuity of velocities ($r = R$)

$$u_r'^{(L)} = u_r'^{(G)}, \quad (4a)$$

$$u_\theta'^{(L)} = u_\theta'^{(G)}, \quad \text{and} \quad (4b)$$

$$\eta \frac{\mathrm{d}U_z^{(L)}}{\mathrm{d}r} + u_z'^{(L)} = \eta \frac{\mathrm{d}U_z^{(G)}}{\mathrm{d}r} + u_z'^{(G)}. \quad (4c)$$

Continuity of axial shear stress ($r = R$)

$$\mu_G\left(\eta \frac{\mathrm{d}^2 U_z^{(G)}}{\mathrm{d}r^2} + \frac{\partial u_z'^{(G)}}{\partial r} + \frac{\partial u_r'^{(G)}}{\partial z}\right) = \mu_L\left(\eta \frac{\mathrm{d}^2 U_z^{(L)}}{\mathrm{d}r^2} + \frac{\partial u_z'^{(L)}}{\partial r} + \frac{\partial u_r'^{(L)}}{\partial z}\right). \quad (4d)$$

Continuity of azimuthal shear stress ($r = R$)

$$\mu_G\left(\frac{\partial u_\theta'^{(G)}}{\partial r} + \frac{1}{r}\frac{\partial u_r'^{(G)}}{\partial \theta} - \frac{u_\theta'^{(G)}}{r}\right) = \mu_L\left(\frac{\partial u_\theta'^{(L)}}{\partial r} + \frac{1}{r}\frac{\partial u_r'^{(L)}}{\partial \theta} - \frac{u_\theta'^{(L)}}{r}\right). \quad (4e)$$

Jump in normal stress ($r = R$)

$$\begin{aligned}&\left(-p'^{(G)} + 2\mu_G \frac{\partial u_r'^{(G)}}{\partial r}\right) - \left(-p'^{(L)} + 2\mu_L \frac{\partial u_r'^{(L)}}{\partial r}\right)\\ &= -\gamma\left(\frac{\eta}{r^2} + \frac{1}{r^2}\frac{\partial^2 \eta}{\partial \theta^2} + \frac{\partial^2 \eta}{\partial z^2}\right), \quad (4f)\end{aligned}$$

where γ is the surface tension coefficient, μ_L and μ_G are the dynamic viscosity of liquid and gas, respectively, and η is the interfacial displacement with respect to the undisturbed jet radius, R. The interfacial displacement obeys the following kinematic condition

$$\text{Kinematic condition:} \quad \frac{D\eta}{Dt} = u_r'. \quad (5)$$

2.3. Normal mode decomposition

To proceed with the calculation of perturbation growth rate, a normal mode decomposition [7] of the flow fields is employed. This implies that the perturbation fields are expressed as,

$$\begin{aligned}&\left[u_r', u_\theta', u_z', p'\right](r,\theta,z,t)\\ &= \left[\hat{u}_r(r), \hat{u}_\theta(r), \hat{u}_z(r), \hat{p}(r)\right]\exp[i(kz + m\theta - \omega t)], \quad (6)\end{aligned}$$

where $\hat{u}_r$, $\hat{u}_\theta$, $\hat{u}_z$ and $\hat{p}$ are functions of the radial direction, k is the complex wavenumber, ω is the frequency and m represents the azimuthal wavenumber. The value of m takes the value 0 for axisymmetric disturbances and 1 for asymmetric disturbances. Spatial analysis is considered, where $\omega = \omega_R \in \mathbb{R}$ and $k = (k_R + ik_I) \in \mathbb{C}$. The complex part of the wavenumber, k_I represents the growth or decay of the disturbance as we move forward in space, i.e. in z.

Substituting the normal mode representation (Eq. (6)) into Eqs. (2), (3), and (4) transforms the governing equations, boundary conditions and interfacial conditions, into ordinary differential equations. Further, the radial component of the perturbations, wavenumber and frequency are non-dimensionalized resulting in $\tilde{u}_r(r)$, $\tilde{u}_\theta(r)$, $\tilde{u}_z(r)$, $\tilde{p}(r)$, $\tilde{k}$, and $\tilde{\omega}$ respectively, using the liquid density, ρ_L, jet velocity U_{jet}, and the jet radius R. The radial coordinate corresponding to the either liquid or gas domains is made to vary between $[-1, 1]$ through the transformation from the original radial coordinate (r) given by

$$\begin{aligned}\tilde{r}_L &= 2\frac{r}{R} - 1 \quad \text{for} \quad r \in [0, R] \quad \text{and}\\ \tilde{r}_G &= 2\frac{r - R}{H - R} - 1 \quad \text{for} \quad r \in [R, H].\end{aligned} \quad (7)$$

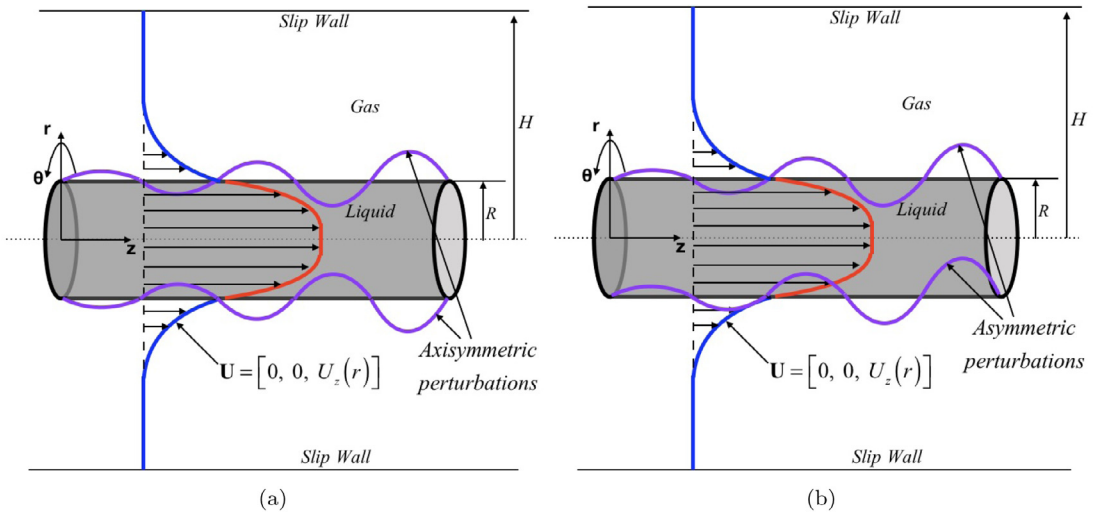

Fig. 1. Schematic representation of the problem set-up with (a) axisymmetric perturbation and (b) asymmetric perturbation.

The final system of non-dimensional ODEs in the liquid domain in the transformed coordinate ($\tilde{r}_{L,G}$) are given by

$$\text{(Continuity)}\quad 2\frac{\mathrm{d}\tilde{u}_r^{(L)}}{\mathrm{d}\tilde{r}_L}+\frac{2}{(\tilde{r}_L+1)}\tilde{u}_r^{(L)}+i\frac{2m}{(\tilde{r}_L+1)}\tilde{u}_\theta^{(L)}+i\tilde{k}\tilde{u}_z^{(L)}=0, \tag{8a}$$

$$\begin{aligned}&(r\text{-mom})\quad -i\tilde{\omega}\tilde{u}_r^{(L)}+i\tilde{k}\tilde{U}_z^{(L)}\tilde{u}_r^{(L)}=-2\frac{\mathrm{d}\tilde{p}^{(L)}}{\mathrm{d}\tilde{r}_L}+\\&\frac{1}{Re}\left[4\frac{\mathrm{d}^2\tilde{u}_r^{(L)}}{\mathrm{d}\tilde{r}_L^2}+\frac{4}{(\tilde{r}_L+1)}\frac{\mathrm{d}\tilde{u}_r^{(L)}}{\mathrm{d}\tilde{r}_L}\right.\\&\left.-\left(\frac{4(m^2+1)}{(\tilde{r}_L+1)^2}+\tilde{k}^2\right)\tilde{u}_r^{(L)}-i\frac{8m}{(\tilde{r}_L+1)^2}\tilde{u}_\theta^{(L)}\right],\end{aligned} \tag{8b}$$

$$\begin{aligned}&(\theta\text{-mom})\quad -i\tilde{\omega}\tilde{u}_\theta^{(L)}+i\tilde{k}\tilde{U}_z^{(L)}\tilde{u}_\theta^{(L)}=-i\frac{2m}{(\tilde{r}_L+1)}\tilde{p}^{(L)}+\\&\frac{1}{Re}\left[4\frac{\mathrm{d}^2\tilde{u}_\theta^{(L)}}{\mathrm{d}\tilde{r}_L^2}+\frac{4}{(\tilde{r}_L+1)}\frac{\mathrm{d}\tilde{u}_\theta^{(L)}}{\mathrm{d}\tilde{r}_L}-\left(\frac{4(m^2+1)}{(\tilde{r}_L+1)^2}+\tilde{k}^2\right)\tilde{u}_\theta^{(L)}\right.\\&\left.+i\frac{8m}{(\tilde{r}_L+1)^2}\tilde{u}_r^{(L)}\right],\quad\text{and}\end{aligned} \tag{8c}$$

$$\begin{aligned}&(z\text{-mom})\quad -i\tilde{\omega}\tilde{u}_z^{(L)}+2\frac{\mathrm{d}\tilde{U}_z^{(L)}}{\mathrm{d}\tilde{r}_L}\tilde{u}_r^{(L)}+i\tilde{k}\tilde{U}_z^{(L)}\tilde{u}_z^{(L)}\\&=-i\tilde{k}\tilde{p}^{(L)}\\&+\frac{1}{Re}\left[4\frac{\mathrm{d}^2\tilde{u}_z^{(L)}}{\mathrm{d}\tilde{r}_L^2}+\frac{4}{(\tilde{r}_L+1)}\frac{\mathrm{d}\tilde{u}_z^{(L)}}{\mathrm{d}\tilde{r}_L}-\left(\frac{4m^2}{(\tilde{r}_L+1)^2}+\tilde{k}^2\right)\tilde{u}_z^{(L)}\right].\end{aligned} \tag{8d}$$

A corresponding set of equations for the gas phase is also obtained. The final interfacial constraints after the radial transformation are given by

(Continuity of velocities)

$$\left[\tilde{u}_r^{(G)}\right]_{\tilde{r}_G=-1}=\left[\tilde{u}_r^{(L)}\right]_{\tilde{r}_L=+1}. \tag{9a}$$

$$\left[\tilde{u}_\theta^{(G)}\right]_{\tilde{r}_G=-1}=\left[\tilde{u}_\theta^{(L)}\right]_{\tilde{r}_L=+1}. \tag{9b}$$

$$\begin{aligned}&\left[\frac{2}{(l-1)}\frac{\mathrm{d}\tilde{U}_z^{(G)}}{\mathrm{d}\tilde{r}_G}\tilde{u}_r^{(G)}+\left(i\tilde{k}\tilde{U}_z^{(G)}-i\tilde{\omega}\right)\tilde{u}_z^{(G)}\right]_{\tilde{r}_G=-1}\\&=\left[2\frac{\mathrm{d}\tilde{U}_z^{(L)}}{\mathrm{d}\tilde{r}_L}\tilde{u}_r^{(L)}+\left(i\tilde{k}\tilde{U}_z^{(L)}-i\tilde{\omega}\right)\tilde{u}_z^{(L)}\right]_{\tilde{r}_L=+1}.\end{aligned} \tag{9c}$$

(Continuity of axial shear stress)

$$\begin{aligned}&n_\mu\left[\left(\frac{4}{(l-1)^2}\frac{\mathrm{d}^2\tilde{U}_z^{(G)}}{\mathrm{d}\tilde{r}_G^2}-\tilde{k}^2\tilde{U}_z^{(G)}+\tilde{k}\tilde{\omega}\right)\tilde{u}_r^{(G)}\right.\\&\left.+\frac{2}{(l-1)}\left(i\tilde{k}\tilde{U}_z^{(G)}-i\tilde{\omega}\right)\frac{\mathrm{d}\tilde{u}_z^{(G)}}{\mathrm{d}\tilde{r}_G}\right]_{\tilde{r}_G=-1}\\&=\left[\left(4\frac{\mathrm{d}^2\tilde{U}_z^{(L)}}{\mathrm{d}\tilde{r}_L^2}-\tilde{k}^2\tilde{U}_z^{(L)}+\tilde{k}\tilde{\omega}\right)\tilde{u}_r^{(L)}+2\left(i\tilde{k}\tilde{U}_z^{(L)}-i\tilde{\omega}\right)\frac{\mathrm{d}\tilde{u}_z^{(L)}}{\mathrm{d}\tilde{r}_L}\right]_{\tilde{r}_L=+1}.\end{aligned} \tag{9d}$$

(Continuity of azimuthal shear stress)

$$\begin{aligned}&n_\mu\left[\frac{1}{(l-1)}\frac{\mathrm{d}\tilde{u}_\theta^{(G)}}{\mathrm{d}\tilde{r}_G}+\frac{1}{(\tilde{r}_G(l-1)+l+1)}im\tilde{u}_r^{(G)}\right.\\&\left.-\frac{1}{(\tilde{r}_G(l-1)+l+1)}\tilde{u}_\theta^{(G)}\right]_{\tilde{r}_G=-1}\\&=\left[\frac{\mathrm{d}\tilde{u}_\theta^{(L)}}{\mathrm{d}\tilde{r}_L}+\frac{1}{(\tilde{r}_L+1)}im\tilde{u}_r^{(L)}-\frac{1}{(\tilde{r}_L+1)}\tilde{u}_\theta^{(L)}\right]_{\tilde{r}_L=+1}.\end{aligned} \tag{9e}$$

(Jump in normal stress)

$$\begin{aligned}&\left[-\tilde{p}^{(G)}+\frac{4n_\mu}{Re(l-1)}\frac{\mathrm{d}\tilde{u}_r^{(G)}}{\mathrm{d}\tilde{r}_G}\right]_{\tilde{r}_G=-1}-\left[-\tilde{p}^{(L)}+\frac{4}{Re}\frac{\mathrm{d}\tilde{u}_r^{(L)}}{\mathrm{d}\tilde{r}_L}\right]_{\tilde{r}_L=+1}\\&=\frac{1}{2We}\left[(-1+m^2+\tilde{k}^2)\frac{\tilde{u}_z^{(G)}-\tilde{u}_z^{(L)}}{\left(\frac{\mathrm{d}\tilde{U}_z^{(L)}}{\mathrm{d}\tilde{r}_L}\Big|_{\tilde{r}_L=+1}-\frac{1}{(l-1)}\frac{\mathrm{d}\tilde{U}_z^{(G)}}{\mathrm{d}\tilde{r}_G}\Big|_{\tilde{r}_G=-1}\right)}\right],\end{aligned} \tag{9f}$$

where $n_\mu=\mu_G/\mu_L$ is the viscosity ratio, $l=H/R$ is the ratio of gas domain extent to the liquid jet radius, and $We=\rho_L U_{jet}^2 R/\gamma$ is

the Weber number. Similarly, the boundary conditions in Eqs. (3) are transformed using Eq. (7).

2.4. Spectral representation

The system given by Eqs. (8) and (9) along with the gas-phase counterpart and boundary conditions are discretized using Chebyshev spectral method [8], where the radial components of the velocity and pressure fields are expressed in terms of Chebyshev polynomials given by

$$\tilde{u}_r^{(L,G)} = \sum_{j=1}^{N_{L,G}+1} a_{r,j-1}^{(L,G)} T_{j-1}\left(\tilde{r}_{L,G}\right), \qquad \tilde{u}_\theta^{(L,G)} = \sum_{j=1}^{N_{L,G}+1} a_{\theta,j-1}^{(L,G)} T_{j-1}\left(\tilde{r}_{L,G}\right), \tag{10a}$$

$$\tilde{u}_z^{(L,G)} = \sum_{j=1}^{N_{L,G}+1} a_{z,j-1}^{(L,G)} T_{j-1}\left(\tilde{r}_{L,G}\right), \quad \text{and} \quad \tilde{p}^{(L,G)} = \sum_{j=1}^{N_{L,G}} a_{p,j-1}^{(L,G)} T_{j-1}\left(\tilde{r}_{L,G}\right), \tag{10b}$$

where T_{j-1} in Eqs. (10) are the Chebyshev polynomials and a_{j-1} are the corresponding coefficients in the Chebyshev expansion.

The liquid and gas domains shown in Fig. 1 are divided into N_L and N_G number of Gauss–Lobatto (G–L) points, respectively. G–L points are projections of equidistant points on a unit semicircle on the x-axis. Hence, G–L points agglomerate near the interface and the boundaries. This leads to a better resolution of the interface by considering less number of G–L points compared to equidistant points. The liquid and gas phase governing equations along with the boundary and interfacial conditions are solved at the G–L points. The system of equations obtained by solving the equations at each G–L point can be represented in matrix form as a non-linear eigenvalue problem in $\tilde{k}$, which is expressed as

$$\tilde{k}^2 \mathbf{C}_2 \cdot \mathbf{a} + \tilde{k}\mathbf{C}_1 \cdot \mathbf{a} + \mathbf{C}_0 \cdot \mathbf{a} = \mathbf{0}. \tag{11}$$

Here $\tilde{k}$ is the eigenvalue, $\mathbf{a} = \left[\mathbf{a}_r^{(L)}, \mathbf{a}_\theta^{(L)}, \mathbf{a}_z^{(L)}, \mathbf{a}_p^{(L)}, \mathbf{a}_r^{(G)}, \mathbf{a}_\theta^{(G)}, \mathbf{a}_z^{(G)}, \mathbf{a}_p^{(G)}\right]^T$ is the eigenvector involving coefficients of Chebyshev expansion given by Eqs. (10) and $(\mathbf{C}_0, \mathbf{C}_1, \mathbf{C}_2)$ are the coefficient matrices. The non-linear eigenvalue problem is linearized using Matrix Companion method [9] as

$$\begin{bmatrix} -\mathbf{C}_1 & -\mathbf{C}_0 \\ \mathbf{I} & \mathbf{0} \end{bmatrix} \cdot \begin{bmatrix} \tilde{k}\mathbf{a} \\ \mathbf{a} \end{bmatrix} - \tilde{k} \begin{bmatrix} \mathbf{C}_2 & \mathbf{0} \\ \mathbf{0} & \mathbf{I} \end{bmatrix} \cdot \begin{bmatrix} \tilde{k}\mathbf{a} \\ \mathbf{a} \end{bmatrix} = \mathbf{0}. \tag{12}$$

The eigenvalues of the discretized system (Eq. (12)) are determined using the QZ-routine in Matlab under the LAPACK library [10]. From the eigenvalues obtained from the QZ algorithm, the spurious eigenvalues are eliminated. The spurious eigenvalues are identified by noting that they become random and do not converge with increasing grid resolution.

The output from the software tool is the eigenvalue $\tilde{k} \in \mathbb{C}$ and the corresponding eigenvector $\mathbf{a} \in \mathbb{C}$ for a given input frequency $\tilde{\omega}_R$. From Eq. (12), we get one set of values of $\tilde{k}$ by writing the equation as $\mathbf{A} \cdot \mathbf{f} - \tilde{k}\mathbf{B} \cdot \mathbf{f}$ where $\mathbf{f}$ is $[\tilde{k}\mathbf{a}; \mathbf{a}]$. Hence, there is only one $\tilde{k}$ but the eigenvectors will be repeated. The first half of eigenvector $\mathbf{f}$ will be k times the second half. We use only one half of the eigenvector to obtain perturbed quantities. The real part of the eigenvalue $\tilde{k}_R$ represents the most unstable wavenumber of the disturbance and the negative part of the complex eigenvalue, $-\tilde{k}_I$, represents the corresponding spatial growth rate. The perturbed quantities $(\tilde{u}_r^{(L,G)}, \tilde{u}_\theta^{(L,G)}, \tilde{u}_z^{(L,G)}, \tilde{p}^{(L,G)})$ are obtained using the eigenvectors $\mathbf{a}$ and substituting them in Eq. (10). These quantities are converted to dimensional form to obtain the perturbed quantities $(\hat{u}_r^{(L,G)}, \hat{u}_\theta^{(L,G)}, \hat{u}_z^{(L,G)}, \hat{p}^{(L,G)})$ in Eq. (6). Hence, for a given input perturbation frequency, the corresponding most unstable wavenumber, its spatial growth rate, and the perturbation flow fields can be determined.

2.5. Base flow field

The base flow field employed is a steady-state field on which the perturbations are imposed. It automatically satisfies continuity and the momentum equations. This base flow has the following form [11]

$$U_L = -U_L^* erf\left(\frac{r-R}{\delta_L}\right) + U_G^* \qquad r \in [0, R], \tag{13a}$$

$$U_G = -U_G^* erf\left(\frac{r-R}{\delta_G}\right) + U_G^* \qquad r \in [R, H], \tag{13b}$$

where the shear layer thicknesses in both liquid and gas are given respectively by δ_L and δ_G. A relation between U_L^* and U_G^* is obtained by the continuity of shear stress at the interface, which is given by

$$U_G^* = \frac{U_{jet}}{\left(1 + \frac{\mu_G}{\mu_L}\frac{\delta_L}{\delta_G}\right)} \quad \text{and} \quad U_L^* = U_{jet} - U_G^*. \tag{14}$$

3. Software architecture

3.1. Software framework

The current code is implemented in MatLab-v2017a and compatible with higher versions. Overall the code is divided into three main scripts along with a validation script, `Validation_Lin_Gordillo.m`, which could be run separately to check the validation plots presented in Section 4. The three scripts are given below:

- `twoPJIT.m` is the main script. It outputs the dispersion plots and the perturbation field for the most unstable mode by calling the `Cylindrical_3D_solution.m` and `perturbation.m`, respectively.
- `Cylindrical_3D_solution.m` discretizes and solves the system of governing equations along with boundary and interfacial conditions.
- `perturbation.m` calls the `Cylindrical_3D_solution.m` function to solve the problem at the most unstable mode and then calculates the corresponding perturbation flow fields.

3.1.1. Input parameters

Input parameters involve fluid and jet properties, the number of G–L points, and the input frequency. This is given in Table 1.

3.1.2. Solution of governing equations

From the given input parameters above, the base flow field is calculated using Eqs. (13) and the coefficient matrices $((\mathbf{C}_0, \mathbf{C}_1, \mathbf{C}_2))$ are obtained. The linearized eigenvalue equation, given by Eq. (12) is solved using the QZ-algorithm to obtain the eigenvalues and eigenvectors. As mentioned in Section 2.4, the spurious eigenvalues are eliminated and the most unstable eigenvalue is chosen from the set of legitimate eigenvalues, and the corresponding eigenvector is determined. The residual error for the solution is monitored to guarantee that the results are accurate.

3.1.3. Post processing and output

The displayed results consist of the growth rate, wavenumber, and residual error for each input frequency. Additionally, the dispersion curves and perturbation flow fields are plotted. Details of these plots are included in Table 2. Also the frequency (ω), wavenumber (k_R), and growth rate $(-k_I)$ corresponding to the most unstable mode will be displayed in the output.

Table 1
Input parameters entered in the code `twoPJIT.m`.

Properties of the jet	Velocity of the liquid jet, U_{jet} in m/s Radius of the jet, R in m Gas domain length, H in m Densities of liquid (ρ_L) and gas (ρ_G) in kg/m^3 Kinematic viscosities of liquid (ν_L) and gas (ν_G) in m^2/s Surface tension coefficient (γ) in N/m Shear layer thicknesses in liquid (δ_L) and gas (δ_G) in m
Mode of disturbance	Axisymmetric ($m = 0$) and Asymmetric ($m = 1$)
Input frequencies	Non-dimensional frequency ($\tilde{\omega}_R$)
Number of G–L points	Number of points in liquid (N_l) Number of points in gas (N_G)

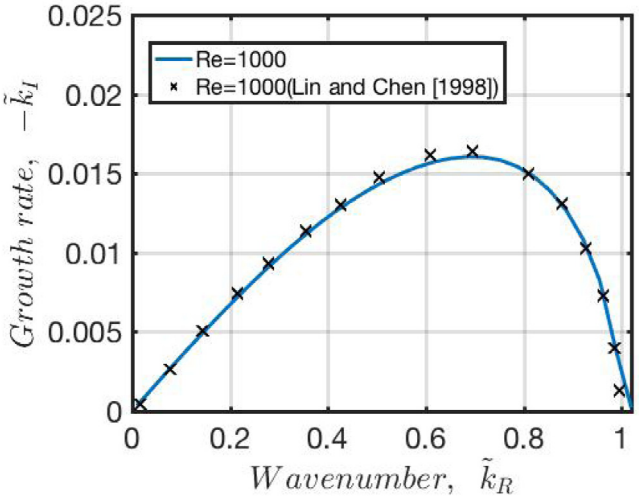

Fig. 2. Dispersion plot validated with [12] for axisymmetric mode with the following properties: $\rho_G/\rho_L = 0.0013$, $\mu_G/\mu_L = 0.018$, Re = 1000, and We = 400.

Table 2
Output plots.

Dispersion plots	**Non-dimensional plots:** Growth rate, $-\tilde{k}_I$ **vs** Frequency, $\tilde{\omega}_R$ Growth rate, $-\tilde{k}_I$ **vs** Wavenumber, $\tilde{k}_R$ **Dimensional plots:** Growth rate, $-k_I$ in m^{-1} **vs** Frequency, ω_R in rad/s Growth rate, $-k_I$ in m^{-1} **vs** Wavenumber, k_R in m^{-1}
Perturbation fields	$\lvert\hat{u}_r\rvert$ in m/s **vs** r in m $\lvert\hat{u}_\theta\rvert$ in m/s **vs** r in m $\lvert\hat{u}_z\rvert$ in m/s **vs** r in m $\lvert\hat{p}\rvert$ in N/m^2 **vs** r in m

3.2. Software functionalities

The current code involves the following major functionalities:

- 3D, two-phase cylindrical jets with viscosity and surface tension forces are considered.
- The code can handle both asymmetric and axisymmetric modes.
- Shear layer thickness in both phases can be varied independently. This is important because in most cases the viscosity of both the fluids differs drastically and this leads to a significant change in the shear layer thickness of both phases.
- The code explicitly gives the most unstable mode for a given set of input frequencies.
- The number of G–L points in liquid and gas domains can be varied independently.

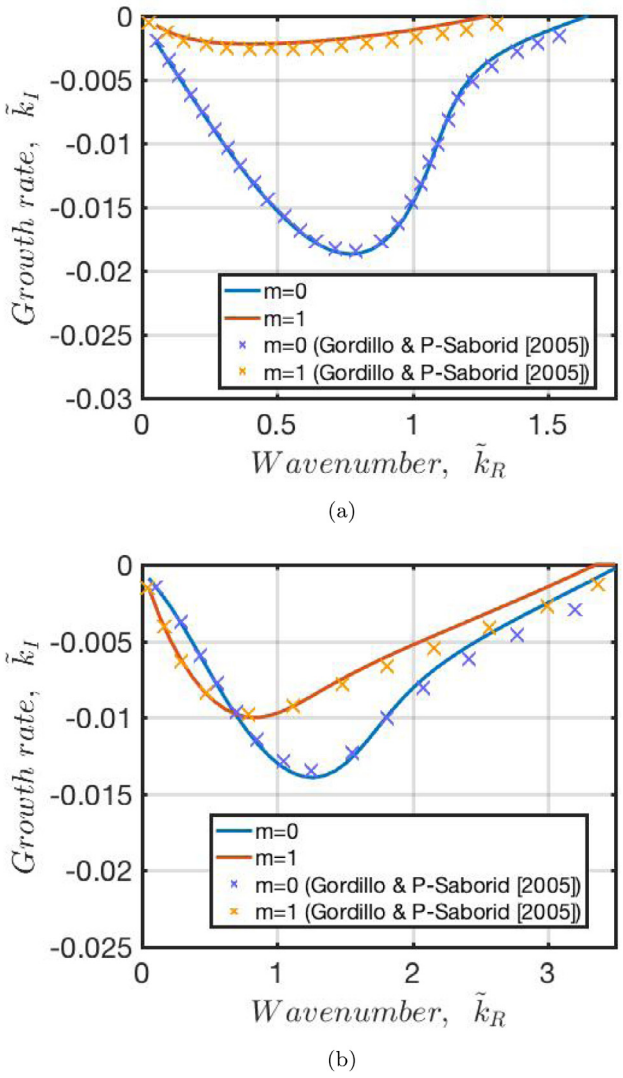

Fig. 3. Dispersion plot validated with [7], with $\rho_G/\rho_L = 0.0012$ and $\mu_G/\mu_L = 0.018$, for both axisymmetric and asymmetric modes for two different Reynolds and Weber numbers (a) Re = 1010, We = 450 and (b) Re = 3367, We = 5000.

4. Validation

The code is validated against predictions published in [12], as shown in Fig. 2, in which a quadratic profile was used for the base velocity with an axisymmetric disturbance. For this validation exercise the present code was changed from its original error function to the quadratic profile. Another validation case involves both axisymmetric and asymmetric modes considered by [7]. In

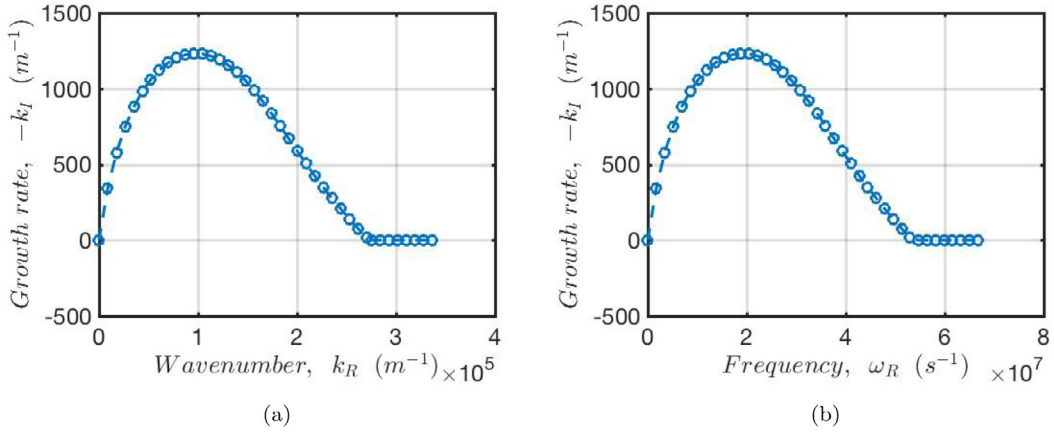

Fig. 4. Dispersion plots for axisymmetric modes ($m = 0$): (a) spatial growth rate versus wavenumber and (b) spatial growth rate versus frequency.

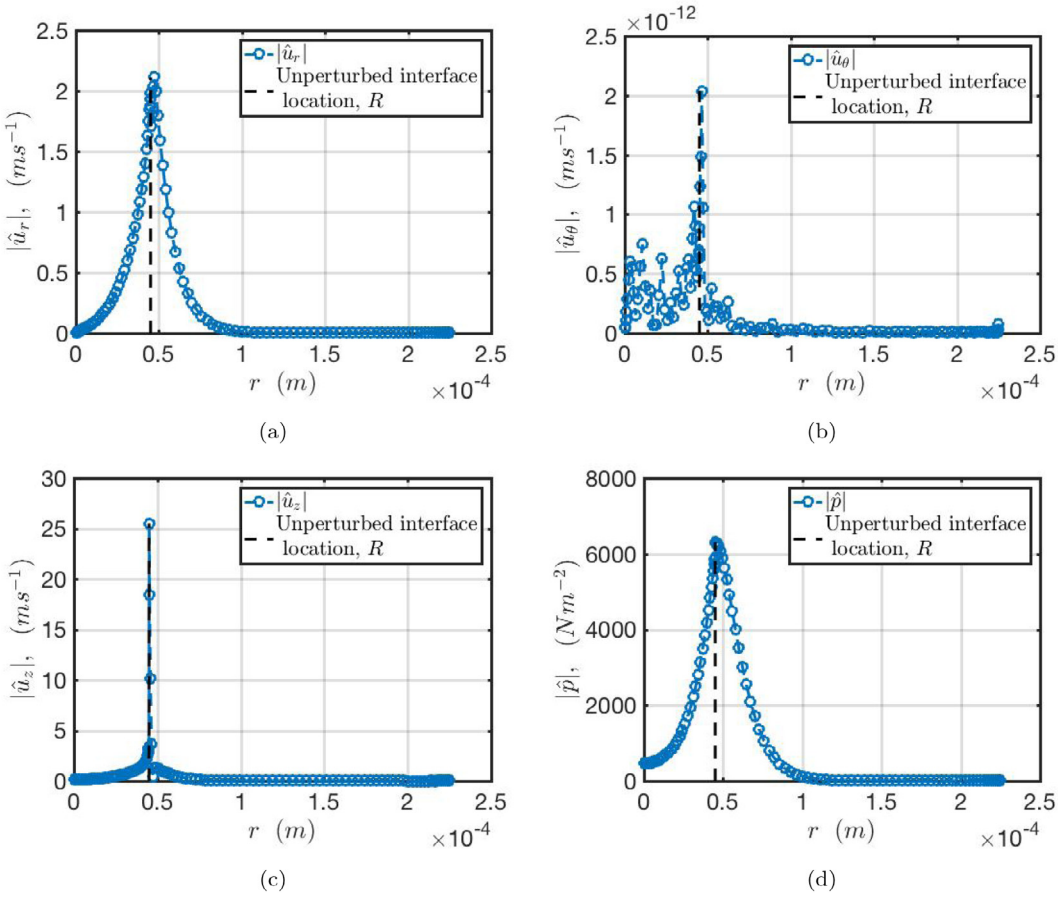

Fig. 5. Perturbation flow field (a) radial component, (b) azimuthal component, (c) axial component and (d) pressure. Note that the value of azimuthal components is very low. This is because of the axisymmetric ($m = 0$) mode where the azimuthal dependence is negligible.

this work, base velocity is constant in the liquid phase, and in the gaseous phase, it is treated by an error function profile. Since these cases involve different base velocity profiles, a separate matlab script, `Validation_Lin_Gordillo.m`, is provided in order to reproduce the results. The results are shown in Fig. 3. From the comparisons (Figs. 2 and 3), it can be stated that good agreement with published data is achieved with the `2PJIT` tool.

5. Illustrative example

The example considered is a two-phase cylindrical flow with Diesel–air conditions as shown in Table 3. The radius (R) and velocity of the liquid jet (U_{jet}) considered for the analysis are 45 μm and 200 m/s, respectively. The boundary layer thicknesses are $\delta_L = R/5$ and $\delta_G = R$, respectively, where Eq. (13) is used to described the base flow profile.

In the execution of `twoPJIT.m` the following information is entered:

- The first prompt involves the mode of instability (axisymmetric or asymmetric). For axisymmetric mode, the value will be 0 and for asymmetric mode the value will be 1. In the current example axisymmetric mode is considered.

Table 3
Fluid properties for the Diesel–Air example.

Phase	ρ (kg/m^3)	μ/ρ (m^2/s)	γ (N/m)
Liquid	666.7	6.947×10^{-7}	0.02
Gas	50	3.76×10^{-7}	

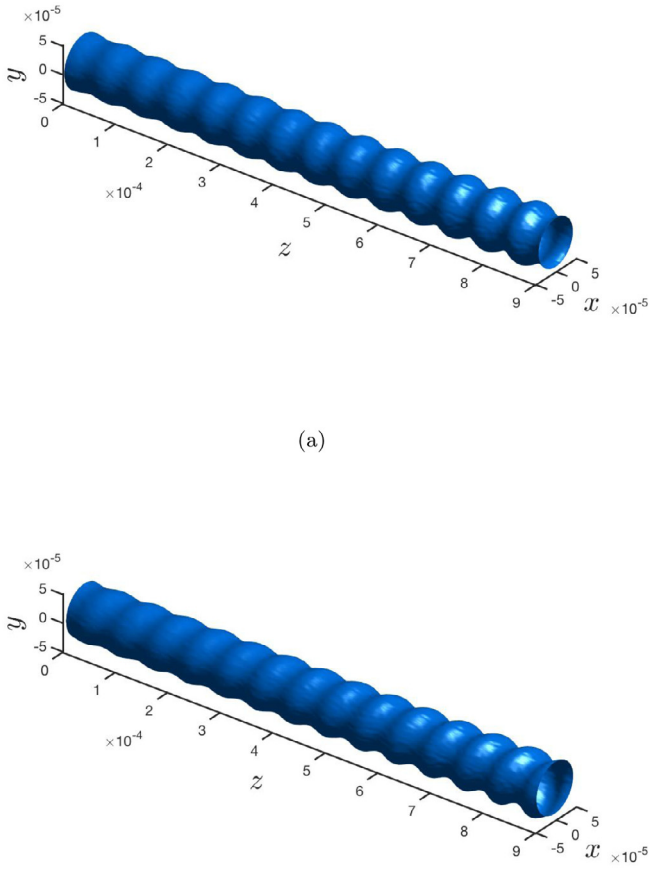

(a)

(b)

Fig. 6. 3D plot of the disturbed jet corresponding to the highest growth rate: (a) axisymmetric perturbation and (b) asymmetric perturbation.

- The second prompt requests values of non-dimensional frequencies ($\tilde{\omega}_R$). This is entered using 'linspace' or 'logspace' function. A single value of ($\tilde{\omega}_R$) also can be given as input. In the current example *linspace*(0, 15, 40) is given as the input $\tilde{\omega}_R$.
- The third prompt is for the number of G–L points to be considered in the liquid domain. The default value is 40.
- The fourth prompt is for the number of G–L points to be considered in the gas domain. The default value is 70.

For each value of $\tilde{\omega}_R$ entered, the code predicts the growth rate ($-\tilde{k}_I$) and wavenumber ($\tilde{k}_R$). It also provides the residual error for the linearized eigenvalue problem in Eq. (12), by considering the L_2 norm as given by Eq. (15). Subsequently, an option is presented to the user for choosing between the non-dimensional dispersion plots or dimensional dispersion plots. The dimensional dispersion plots obtained for the given example are shown in Fig. 4.

$$\text{Residual Error} = \left\| \begin{bmatrix} -\mathbf{C}_1 & -\mathbf{C}_0 \\ \mathbf{I} & \mathbf{0} \end{bmatrix} \cdot \begin{bmatrix} \tilde{k}\mathbf{a} \\ \mathbf{a} \end{bmatrix} - \tilde{k} \begin{bmatrix} \mathbf{C}_2 & \mathbf{0} \\ \mathbf{0} & \mathbf{I} \end{bmatrix} \cdot \begin{bmatrix} \tilde{k}\mathbf{a} \\ \mathbf{a} \end{bmatrix} \right\| \tag{15}$$

Table 4
Convergence of eigenvalues with N_G ($N_L = 40$)

N_G	Eigenvalue ($\tilde{k}$)
40	$4.3083 + i0.055539$
50	$4.3085 + i0.05542$
60	$4.3084 + i0.055428$
70	$4.3085 + i0.055424$

Table 5
Convergence of eigenvalues with N_L ($N_G = 70$)

N_L	Eigenvalue ($\tilde{k}$)
10	$4.3085 + i0.055416$
20	$4.3085 + i0.055424$
30	$4.3085 + i0.055424$
40	$4.3085 + i0.055424$

The point with the highest growth rate in a given dispersion curve is the most unstable mode. The frequency, wavenumber, and the growth rate of the most unstable mode are displayed on the screen, which in this case are 18.803×10^6 rad/s, 95743 m^{-1}, and 1232 m^{-1}, respectively.

The convergence of eigenvalues ($\tilde{k}$) are tabulated in Tables 4 and 5. It can be observed that the $\tilde{k}$ converges when the number of G–L points are 70 in gas (Table 4) and 40 in liquid (Table 5) respectively. Since the height of the gas domain ($H - R$) is greater than the liquid jet radius (R), more G–L points would be required in the gas domain compared to the liquid domain for convergence.

The perturbed flow field is obtained directly from the eigenvector, $\mathbf{f}$, corresponding to the most unstable eigenvalue. As described previously in Section 2.4, this eigenvector is a solution of $\mathbf{A}\cdot\mathbf{f} - \tilde{k}\mathbf{B}\cdot\mathbf{f}$; thus, for any arbitrary constant, c, $c\mathbf{f}$ is also a solution to the generalized eigenvalue problem. To avoid this ambiguity, $\mathbf{f}$ is fixed by imposing that the radial velocity at the interface is set to a fixed value corresponding to 1% of the injection velocity, U_{jet}. This change has the added benefit that as the numerical resolution is changed, the associated eigenvectors are anchored to a specific value. Thus, numerically convergence can also be checked with respect to this eigenvector. The perturbation flow fields $\left(|\hat{u}_r|, |\hat{u}_\theta|, |\hat{u}_z|, |\hat{p}|\right)$ are plotted with respect to the radial position, r, as shown in Fig. 5. To provide a 3D visualization of the jet surface with the perturbations corresponding to the highest growth rate, an image is included in Fig. 6. For the sake of comparison, an asymmetric disturbance ($m = 1$) is also shown. In both images, the growth of the instability is observed as a function of the axial coordinate, z.

6. Impact

The 2PJIT tool fills a gap in the existing literature by providing a software tool for the analysis of hydrodynamic instabilities in 3D cylindrical jets. These types of jets generally characterize the injection of liquids in various applications, including liquid cooling of microelectronics, fuel injection, agricultural sprays, post-combustion after-treatment strategies, among various heat transfer applications. The 2PJIT predicts the growth of instabilities of these jets and thus provides information on how the critical hydrodynamic breakup process of the liquid eventually leads to droplet creation and spray formation. Other alternatives in predicting the growth of instabilities are offered by highly-resolved computational fluid dynamics simulations, which are orders of magnitude more computationally expensive than 2PJIT. However, since there are no open-source codes available to the author's knowledge, which considers a general two-phase cylindrical geometry, the 2PJIT tool helps fill this need.

7. Conclusions

The main objective of the 3D, two-phase jet instability tool (2PJIT) is to provide a generalized tool to analyze the spatial stability of normal modes observed in two-phase shear flows involving cylindrical coordinates. As opposed to various works in the literature, in the present tool viscosity is considered in both phases as well as surface tension. Using this tool, the unstable perturbation modes, their frequency, wavenumber, and growth rate can be predicted for arbitrary jet conditions.

Declaration of competing interest

The authors declare that they have no known competing financial interests or personal relationships that could have appeared to influence the work reported in this paper.

Acknowledgments

The support from the National Science Foundation, USA (Number 1703825) is gratefully acknowledged with Ron Joslin its program director.

References

[1] Miesen R, Boersma BJ. Hydrodynamic stability of a sheared liquid film. J Fluid Mech 1995;301:175–202.
[2] Young W, Wolfe C. Generation of surface waves by shear-flow instability. J Fluid Mech 2014;739:276–307.
[3] Lin S, Reitz R. Drop and spray formation from a liquid jet. Ann Rev Fluid Mech 1998;30(1):85–105.
[4] Lefebvre AH, McDonell VG. Atomization and sprays. Chemical Rubber Company Press; 2017.
[5] Rayleigh L. On the instability of jets. Proc Lond Math Soc 1878;1(1):4–13.
[6] Schmid PJ, Henningson DS. Stability and transition in shear flows. Appl Mech Rev 2001;B57–9.
[7] Gordillo J, Pérez-Saborid M. Aerodynamic effects in the break-up of liquid jets: on the first wind-induced break-up regime. J Fluid Mech 2005;541:1–20.
[8] Boyd JP. Chebyshev and fourier spectral methods. Courier Corporation; 2001.
[9] Bridges T, Morris PJ. Differential eigenvalue problems in which the parameter appears nonlinearly. J Comput Phys 1984;55(3):437–60.
[10] Anderson E, Bai Z, Bischof C, Demmel J, Dongarra J, Croz JD, et al. LAPACK users' guide. Society for Industrial and Applied Mathematics; 1999.
[11] Yecko P, Zaleski S, Fullana J-M. Viscous modes in two-phase mixing layers. Phys Fluids 2002;14(12):4115–22.
[12] Lin S, Chen J. Role played by the interfacial shear in the instability mechanism of a viscous liquid jet surrounded by a viscous gas in a pipe. J Fluid Mech 1998;376:37–51.